Materials Advances

ROYAL SOCIETY OF CHEMISTRY

PAPER

View Article Online
View Journal | View Issue

Cite this: *Mater. Adv.*, 2025, 6, 345

D–A–D type high contrast mechanochromic luminescence based on anthracene and pyridinium salt derivatives†

Xianchen Hu, Zhengfen Liu, Shubiao Xiao * and Junli Yang *

Fluorescent color-changing smart materials based on force stimulus have attracted wide attention due to their multifunctional and reversible characteristics, leading to advanced applications. However, it is still challenging to develop high-contrast mechanochromic luminescent molecules and reveal the relationship between their structure and properties. This article illustrates the high-contrast mechanochromic properties of D–A–D type derivatives. Two pyridine-functionalized anthracene derivatives (**MTPA** and **BTPA**) both showed significant photoluminescence shift under mechanical force stimulus. It is worth noting that the unilaterally substituted D–A–D anthracene derivative (**MTPA**) exhibits a significant wavelength shift of 122 nm when ground, and the luminescence color changes from blue to yellow. Moreover, it can recover to the original luminescent color after steaming with water or ethanol. This study not only elucidates the mechanochromic properties of D–A–D type cationic organic small molecules, but also provides a novel design concept for designing high-contrast mechanochromic materials.

Received 9th October 2024,
Accepted 29th November 2024

DOI: 10.1039/d4ma01015a

rsc.li/materials-advances

Introduction

As an attractive "smart" stimulus-responsive solid-state material, mechanochromic luminescent (MCL) materials can exhibit significant changes in luminescent color under external mechanical stimuli (such as grinding, cutting, compression and stretching), and can usually be restored to the original luminescent color by solvent fumigation, heating and other methods after the external force is removed, showing dynamic and reversible solid-state luminescent color changes.[1–6] In addition, since force is a simple and easy-to-achieve external stimulus method, and the luminescent color changes accompanied by the change of force could be directly observed by the naked eye, this smart luminescent material has been widely used in data storage, anti-counterfeiting, security inks and memory recording devices.[7–10]

In recent years, scientists have reported a variety of organic MCL molecules, such as tetraphenylethylene,[11,12] triphenylamine,[13,14] carbazole,[15,16] spiropyran derivatives,[17,18] and others.[19–23] Although there have been some design strategies for MCL molecules reported so far, such as doping,[24,25] polymer,[26] intermolecular noncovalent interactions,[27,28] donor–acceptor compounds,[29,30] and the site effect of substituents,[31,32] *etc.*, there are still many uncertainties regarding the relationship between the molecular structure and the properties of MCL. In addition, due to the limitations of molecular structure, most MCL materials exhibit relatively limited ranges of emission wavelength changes and low sensitivity to mechanical forces when subjected to mechanical stress, which greatly limits their practical applications.[1,33] In recent years, researchers have reported a small number of molecules that exhibit wavelength shifts greater than 100 nm under mechanical force. Due to the significance and reversibility of their luminescent color changes, these molecules have demonstrated broad application prospects in fields such as high-level anti-counterfeiting, ion probes, and imaging, *etc.*[24,34–36] Therefore, it remains a challenging task to construct new high-contrast MCL materials using pure organic fluorescent groups and reveal the relationship between their structures and properties.

Donor–acceptor (D–A) molecules represent a class of molecules with unique luminescent properties, whose luminescent mechanism mainly relies on the interactions between electron donors and acceptors. This interaction could induce intramolecular charge transfer, leading to the formation of excited states and the generation of luminescence.[37,38] By precisely designing the structures of donors and acceptors and the torsion angles between them, the electronic structure and energy state of the molecules could be adjusted, thereby effectively controlling their luminescent properties.[39,40] Moreover, studies have shown that D–A molecules with significant intramolecular charge transfer (ICT) properties possess ideal

Yunnan Key Laboratory of Crystalline Porous Organic Functional Materials, College of Chemistry and Environmental Science, Qujing Normal University, Qujing 655011, China. E-mail: yangjlili@sina.com, xiashubiao401@163.com

† Electronic supplementary information (ESI) available. See DOI: https://doi.org/10.1039/d4ma01015a

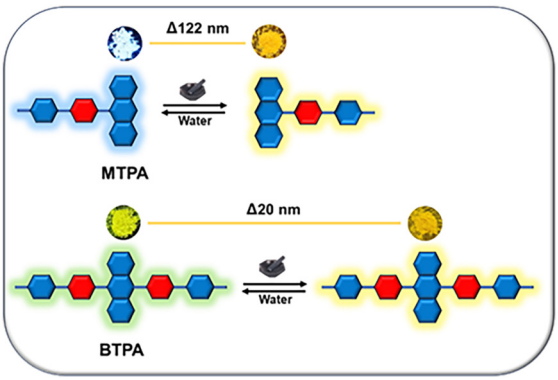

Scheme 1 Schematic diagram of the MCL of **MTPA** and **BTPA**.

solid-state luminescent characteristics.[41,42] Anthracene and its derivatives, classified as a class of efficient luminescent molecules, exhibit not only unique fluorescence and phosphorescence properties, but also modifiable structures, making them promising candidates for a wide range of applications in the field of luminescence.[43–48] Although there have been some reports on the MCL properties of anthracene and its derivatives, most anthracene derivatives only exhibited slight changes in luminescent color under mechanical stress.[49–51]

Inspired by the luminescent mechanism of D–A molecules, and the reported examples of MCL protonated pyridine rings,[4,52,53] we designed and synthesized two cationic MCL molecules (**MTPA**[54] and **BTPA**[55]) by organically combining anthracene as the electron donor and pyridinium salt as the electron acceptor. Both molecules exhibited strong luminescent properties in the solid state. Interestingly, both molecules exhibited different MCL changes (Scheme 1), which were reversible interconversion processes. Among them, the D–A–D type **MTPA** molecule exhibited high-contrast MCL behavior, with a significant change in emission wavelength before and after grinding (emission wavelength change of 122 nm, the luminescent color from blue to yellow). Theoretical calculations and experimental results confirmed that the phase transition and planarization of the conformation of molecules under grinding were the main reasons for the redshift of the emission of **MTPA** and **BTPA** molecules, and the greater change in the emission wavelength ($\Delta\lambda$) of **MTPA** under external mechanical stimulation may be attributed to the smaller steric hindrance effect of the unilateral pyridine group, which makes its ordered stacking structure easier to be destroyed by external forces.

Results and discussion

The compounds **MTPA** and **BTPA** were synthesized by using the route shown in Schemes S1 and S2 (ESI†). The compounds were characterized by ^{1}H NMR. Relevant data and information are shown in the ESI† (Fig. S6–S11).

Photophysical properties of MTPA and BTPA

To investigate the optical properties of the target compounds, we measured the normalized UV-Vis absorption spectra and fluorescence spectra of **MTPA** and **BTPA** in distilled water at room temperature ([**MTPA**] = 2.0 × 10^{-5} M, [**MTPA**] = 2.0 × 10^{-5} M), and the results are shown in Fig. S1 and S2 (ESI†). The spectra indicated that the compounds **MTPA** and **BTPA** have three distinct absorption peaks in aqueous solution, with **MTPA** showing absorption peaks at 247 nm, 288 nm, and 417 nm, and **BTPA** showing absorption peaks at 247 nm, 291 nm, and 420 nm (Fig. S1, ESI†). The initial two absorption peaks may be attributed to π–π* transitions, while the latter (417 nm and 420 nm) may be attributed to intramolecular charge transfer (ICT), with corresponding fluorescence emission peaks located at 624 nm and 587 nm (Fig. S2, ESI†). Subsequently, the fluorescence emission spectra of **MTPA** and **BTPA** in various polar solvents were measured (Fig. 1). The spectral results

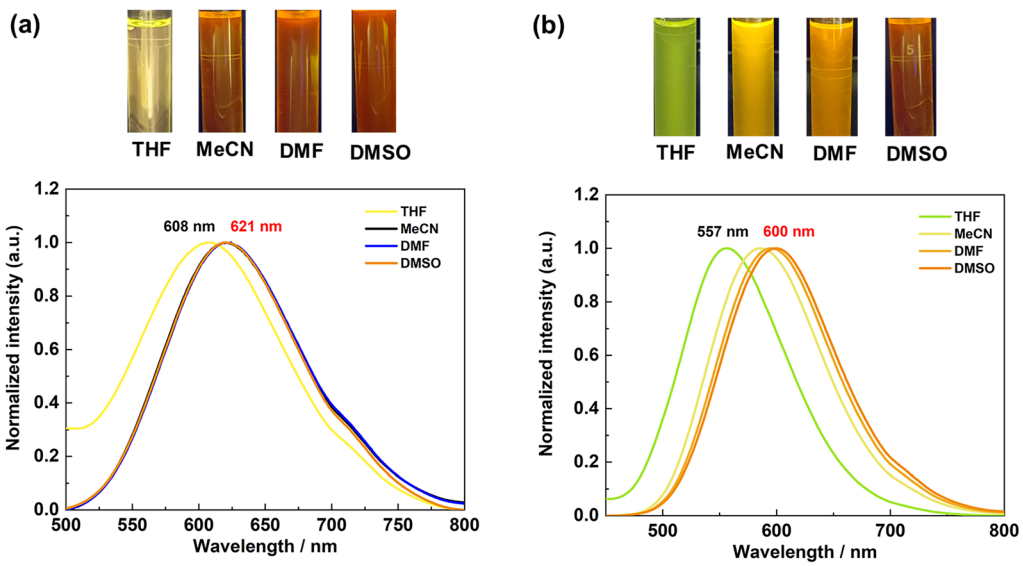

Fig. 1 Photographs (under UV irradiation at 365 nm) and normalized emission spectra (λ_{ex} = 420 nm) for **MTPA** (a) and **BTPA** (b) in various solvents.

showed that both **MTPA** and **BTPA** displayed shorter emission wavelengths (608 nm and 557 nm) in tetrahydrofuran and longer emission wavelengths (621 nm and 600 nm) in dimethyl sulfoxide (DMSO). These observations indicated that **MTPA** and **BTPA** possess solvatochromic properties and exhibited intramolecular charge transfer (ICT) characteristics.[56,57] The fluorescence quantum yields (φ_F) and fluorescence lifetime of **MTPA** and **BTPA** in the solid state were carried out. In the results, we can observe a trend of decreased fluorescence quantum yields for both the **MTPA** and **BTPA** compounds following grinding, compared to their original powder (Table S1, ESI†). Meanwhile, the fluorescence lifetime exhibits a significant enhancement (Table S1 and Fig. S3, ESI†).

Mechanochromic properties of MTPA and BTPA

As illustrated in Fig. 2, the maximum emission wavelength of the original **MTPA** powder was 450 nm (Fig. 2a), and the original powder displayed blue fluorescence under 365 nm UV light irradiation (Fig. 2c). After mechanical grinding of the solid powder of compound **MTPA**, the maximum emission wavelength of **MTPA** red-shifts to 572 nm (Fig. 2a), and the fluorescence emission color changes to yellow (Fig. 2c), demonstrating a significant mechanochromic behavior of **MTPA** ($\Delta\lambda$ = 122 nm). Interestingly, when fumigated with water or ethanol, the grinded (yellow-emitting) **MTPA** could be reverted to its original state (blue-emitting), indicating that **MTPA** exhibits reversible mechanochromic behavior. Similarly to **MTPA**, **BTPA** also demonstrated mechanochromic behavior. The original **BTPA** powder exhibited high fluorescence emission in the solid state, exhibiting green fluorescence at 550 nm (Fig. 2d). Following mechanical grinding, the maximum emission wavelength red-shifts to 570 nm ($\Delta\lambda$ = 20 nm), exhibiting yellow fluorescence. Similarly, under fumigation with water or ethanol, the luminescent color of **BTPA** could also be restored to the initial green fluorescence. These results indicated that both compounds **MTPA** and **BTPA** possess significant force-induced luminescent chromic properties with good reversibility, among which the mechanochromic behavior of **MTPA** was more significant, which may be related to the arrangement and conformation of the molecules.

To investigate the mechanochromic mechanism of **MTPA** and **BTPA**, we analyzed the powder X-ray diffraction (PXRD) patterns of the two compounds before and after grinding. As illustrated in Fig. S4 and S5 (ESI†), the original powders of **MTPA** and **BTPA** both exhibited intense and sharp diffraction peaks, indicating their crystalline structures. After mechanical grinding, the PXRD patterns of **MTPA** and **BTPA**, compared to the initial samples, exhibited several broad diffuse peaks in the diffraction patterns, with a significant decrease in the intensity of the diffraction peaks, indicating that the crystalline structure of the samples was partially destroyed to some extent, and some intermolecular interactions may have disappeared or weakened. After fumigation with water or ethanol, the PXRD patterns of the ground samples were found to be identical to the initial samples, revealing the restoration of their crystal structures, indicating the formation of a crystalline state similar

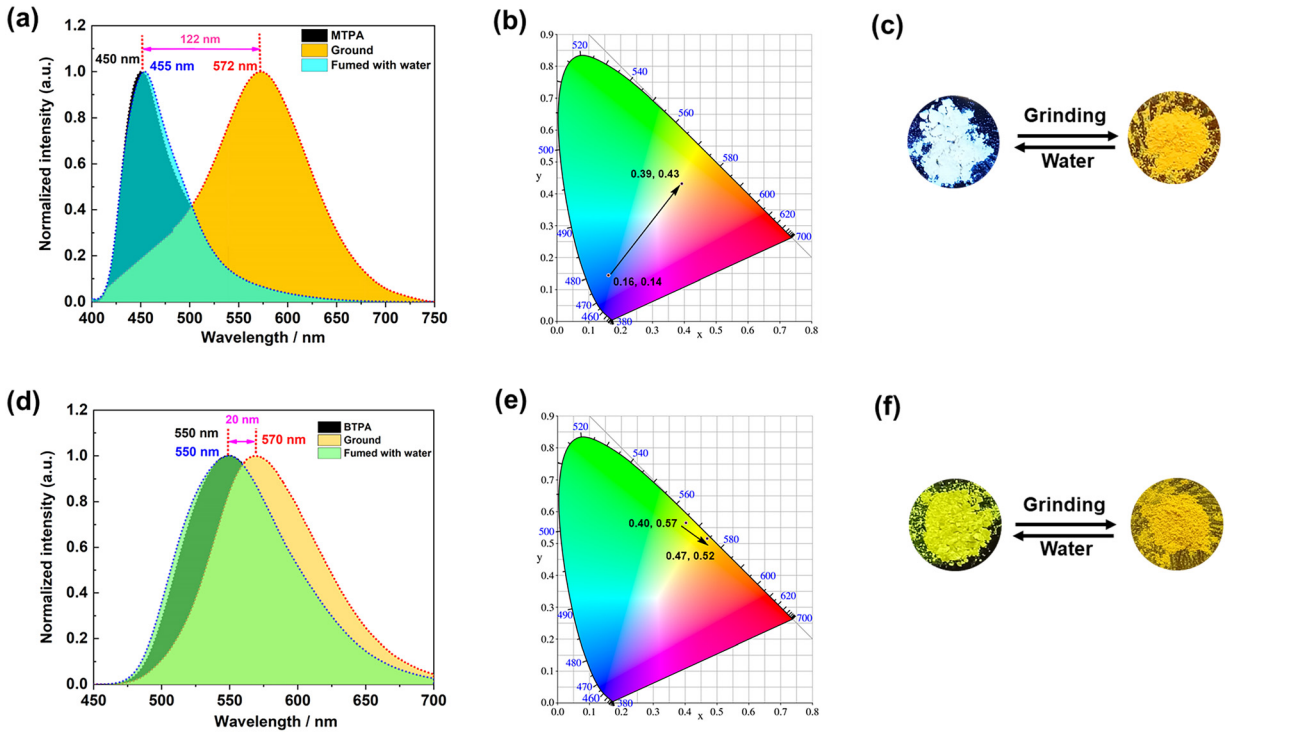

Fig. 2 The MCL behaviors of **MTPA** and **BTPA**. Normalized emission spectra for the as-prepared and ground solids of **MTPA** (λ_{ex} = 380 nm) (a) and **BTPA** (λ_{ex} = 420 nm) (d); the CIE-1931 chromaticity diagrams for the as-prepared and ground solids of **MTPA** (b) and **BTPA** (e); optical images in different solids for **MTPA** (c) and **BTPA** (f) under UV irradiation (365 nm).

to the original powders. Notably, the PXRD diffraction peak intensity and peak broadening of **MTPA** after grinding were significantly greater than those of **BTPA**. This may be attributed to the fact that the crystalline transformations and conformational changes induced by milling in **MTPA** were more pronounced than those in **BTPA**, which was consistent with the spectral chromic results. This suggests that the mechanoresponsive behavior of **MTPA** and **BTPA** was highly correlated with phase transitions, with the compounds transitioning from an original microcrystalline state to an amorphous state after grinding, and then regaining diffraction peaks after fumigation, thus achieving reversible fluorescence transitions.

DFT calculation

To understand the influence of the electronic structure and geometric conformation of **MTPA** and **BTPA** on their optical properties, DFT (density functional theory) calculations were performed. The frontier molecular orbital energy diagrams and the electron cloud distributions for **MTPA** and **BTPA** are shown in Fig. 3. It was observed that the electron densities of the HOMO orbitals of **MTPA** and **BTPA** were predominantly concentrated on the electron-rich anthracene moiety, while the electron cloud densities of the LUMO orbitals of **MTPA** and **BTPA** were distributed on the electron-deficient pyridinium and anthracene segment. This difference in electron cloud density between **MTPA** and **BTPA** suggests the occurrence of ICT from the electron-rich anthracene unit to the electron-deficient pyridinium segment. The calculated results also underscored the existence of donor–acceptor structures. Additionally, the orbital energy levels of the anthracene derivatives were computed and are presented in the inset of Fig. 3. The HOMO energy levels were determined to be −5.64 eV and −5.86 eV, whereas the LUMO energy levels were found to be −2.81 eV and −3.04 eV, respectively. Utilizing the formula for calculating the energy band-gap (E_g = − (LUMO–HOMO)), the values were determined to be 2.83 eV and 2.82 eV. Moreover, the ground-state dipole moments of **MTPA** and **BTPA** were calculated as 7.7778 Debye and 0.0558 Debye, respectively. These results were consistent with the UV-Vis absorption spectra.[58]

Large changes in ground state dipole moments contributed to the enhancement of intramolecular charge transfer. Compared with the centrosymmetric **BTPA**, the axisymmetrically symmetric **MTPA** had lower exciton binding energy and enhanced intermolecular interaction, which contributed to exciton dissociation and improved charge transport. Consequently, **BTPA** showed good force chromism. In addition, from the perspective of the optimized geometric structures of **MPTA** and **BTPA** (Fig. S12, ESI†), the torsion angles between the pyridine groups and the central anthracene groups of **MPTA** and **BTPA** were 60.45° and 65.90°. Although the torsion angle of **MPTA** was smaller than that of **BTPA** in the optimal structure, the centrosymmetric molecular structure of **BTPA** exhibited greater steric hindrance, which was not conducive to the alteration of molecular stacking mode under grinding. Consequently, the spectral change value of **MPTA** under grinding conditions was greater, which was also consistent with the XRD test results.[4]

The application of MTPA and BTPA in a drawing board and information encryption

Inspired by the fact that **MTPA** molecules could achieve high-contrast fluorescence color change under mechanical force

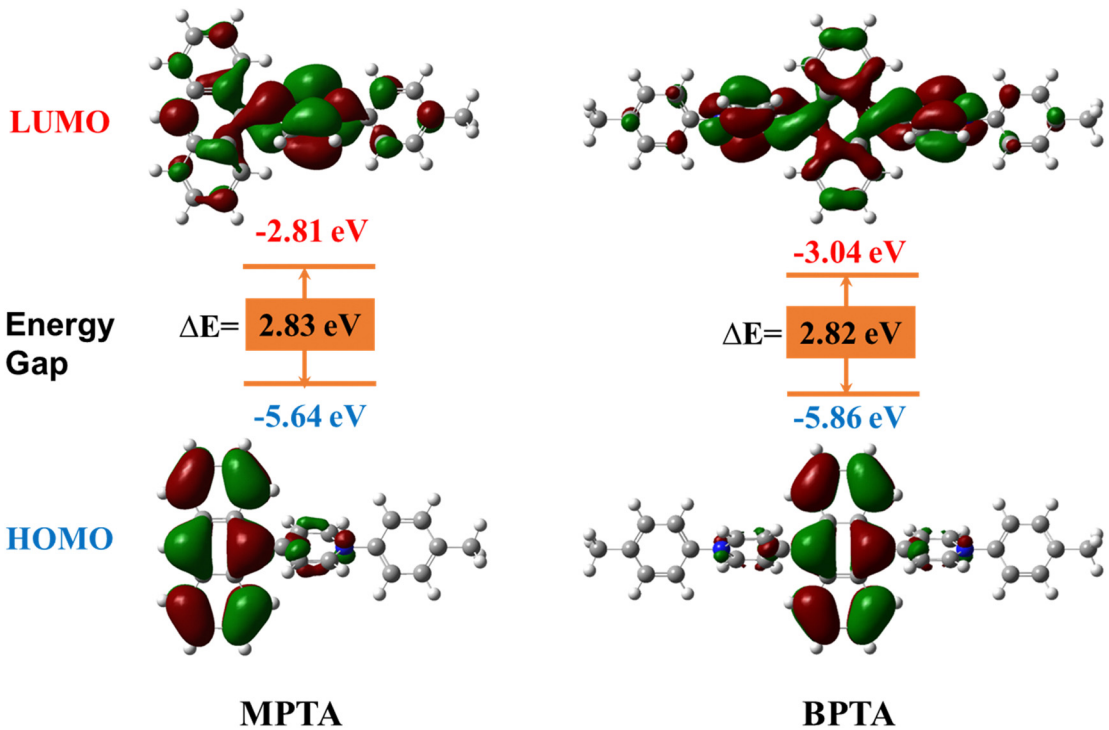

Fig. 3 HOMO/LUMO levels and electron cloud distributions of **MTPA** (left) and **BTPA** (right) compounds.

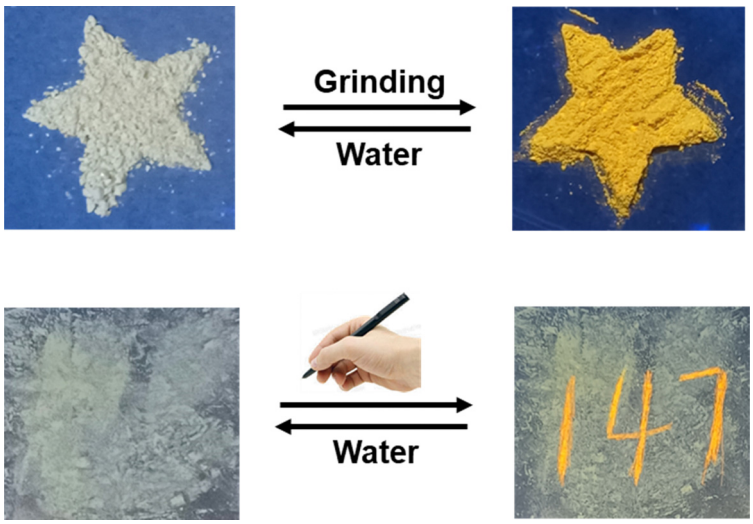

Fig. 4 Reversible color drawing board affixed with **MTPA** powder (under UV-light 365 nm).

stimulation, we have designed a color painting board. Fig. 4 presents a representative experimental result. Firstly, the **MTPA** powder was affixed to the painting board, and then a pen without ink was employed to inscribe on the board. Under the illumination of a 365 nm ultraviolet lamp, the writing could be clearly seen as bright yellow fluorescence. After steaming the written painting board with water vapor, the yellow fluorescence disappeared, thus achieving the development of a reusable color painting board.

Finally, based on the reversible mechanochromic properties and optical responsiveness of **MTPA** and **BTPA**, they were applied to the decryption of Morse code within liquid crystal devices (Fig. 5). As a proof-of-concept diagram, this system features a reversible dual-emission fluorescence output mode. Firstly, the ground **MTPA** and **BTPA** were arranged in an array. Under the influence of water vapor, the system could receive two fluorescence emission signals (λ = 450 nm and 550 nm). Then, different information was obtained by collecting the emission signals from each microgrid within the entire array. Interestingly, after the information was read, the array could be returned to its initial state through simple grinding, thus achieving reversible dual encryption of information. This force and water vapor reversible stimulus-responsive luminescent material constructed from mechanochromic molecular photoswitches has potential application value in the fields of information storage and optical devices.

Conclusions

In summary, we have successfully synthesized two cationic mechanochromic organic small molecules (**MTPA** and **BTPA**),

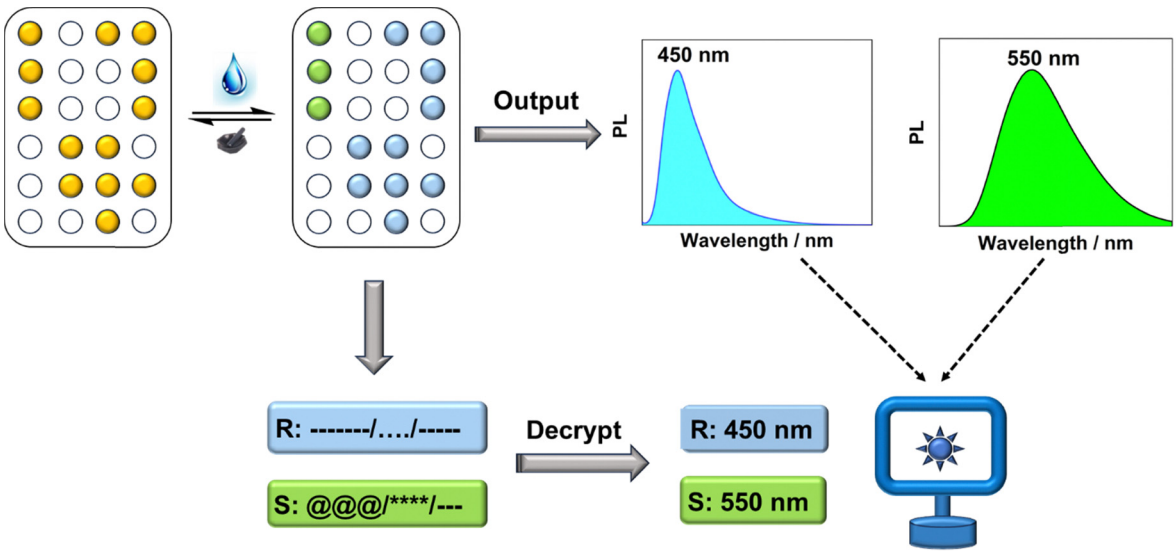

Fig. 5 Encryption and decryption of mechanical color-changing dual-mode information based on **MTPA** and **BTPA**.

both of which demonstrated reversible MCL properties in the solid state. The research results showed that the phase transition and conformational planarization of molecules under mechanical stimulation led to significant red-shifts in the emission spectra of **MTPA** and **BTPA**. Among them, the D–A–D type **MTPA** molecule has a smaller steric hindrance effect of the unilateral pyridine group, making its ordered stacking structure easier to be destroyed by external force, resulting in a wide range of wavelength change ($\Delta\lambda$ = 122 nm) in the emission wavelength before and after grinding. It shows a pronounced high contrast MCL behavior. This study not only contributes to the research on the mechanochromic luminescence mechanism of D–A–D molecules, but also endows MCL materials with potential applications in the field of intelligent anti-counterfeiting.

Author contributions

X. Hu: investigation, spectral testing, writing – original draft, visualization. Z. Liu: synthesis characterization of compounds, investigation, writing – original draft, visualization. S. Xiao: funding acquisition, writing – review & editing. J. Yang: data analysis, supervision, writing – review & editing.

Data availability

The data supporting this study's findings are available from the corresponding author upon reasonable request.

Conflicts of interest

The authors have no conflicts to declare.

Acknowledgements

This work was financially supported by the National Natural Science Foundation of China (No. 22261047), the Special Basic Cooperative Research Innovation Programs of Qujing Science and Technology Bureau & Qujing Normal University (Grant No. KJLH2023YB01), and the Program for Innovative Research Team in Qujing University.

Notes and references

1 Y. Huang, L. Ning, X. Zhang, Q. Zhou, Q. Gong and Q. Zhang, *Chem. Soc. Rev.*, 2024, **53**, 1090–1166.
2 Z. Chi, X. Zhang, B. Xu, X. Zhou, C. Ma, Y. Zhang, S. Liu and J. Xu, *Chem. Soc. Rev.*, 2012, **41**, 3878–3896.
3 R. Kubota, Y. Yuan, R. Yoshida, T. Tachikawa and S. Ito, *Mater. Adv.*, 2022, **3**, 5826–5835.
4 D. Sun, Y. Wu, X. Han and S. Liu, *Nat. Commun.*, 2023, **14**, 4190–4201.
5 H. Traeger, Y. Sagara, D. J. Kiebala, S. Schrettl and C. Weder, *Angew. Chem., Int. Ed.*, 2021, **60**, 16191–16199.
6 N. Xu, W. Xu, M. Sun, Y. Yuan, X. Luan, Y. Wan and H. Wang, *Mater. Adv.*, 2023, **4**, 3645–3653.
7 L. Bai, P. Bose, Q. Gao, Y. Li, R. Ganguly and Y. Zhao, *J. Am. Chem. Soc.*, 2017, **139**, 436–441.
8 W. Zhao, Z. Liu, J. Yu, X. Lu, J. W. Y. Lam, J. Sun, Z. He, H. Ma and B. Z. Tang, *Adv. Mater.*, 2021, **33**, 2006844.
9 W. Li, Q. Huang, Z. Mao, J. Zhao, H. Wu, J. Chen, Z. Yang, Y. Li, Z. Yang, Y. Zhang, M. P. Aldred and Z. Chi, *Angew. Chem., Int. Ed.*, 2020, **59**, 3739–3745.
10 Z. Wen, T. Yang, D. Zhang, Z. Wang, S. Dong, H. Xu, Y. Miao, B. Zhao and H. Wang, *J. Mater. Chem. C*, 2022, **10**, 3396–3403.
11 W. Zhao, Z. He, Q. Peng, J. W. Y. Lam, H. Ma, Z. Qiu, Y. Chen, Z. Zhao, Z. Shuai, Y. Dong and B. Z. Tang, *Nat. Commun.*, 2018, **9**, 3044.
12 Z. Ma, Z. Wang, X. Meng, Z. Ma, Z. Xu, Y. Ma and X. Jia, *Angew. Chem., Int. Ed.*, 2016, **55**, 519–522.
13 C. Zhu, Q. Luo, Y. Shen, C. Lv, S. Zhao, X. Lv, F. Cao, K. Wang, Q. Song, C. Zhang and Y. Zhang, *Angew. Chem., Int. Ed.*, 2021, **60**, 8510–8514.
14 Z. Lv, Z. Man, Z. Xu, L. Fu, S. Li, Y. Zhang and H. Fu, *Adv. Opt. Mater.*, 2021, **9**, 2100598.
15 Y. Chen, A. Li, X. Li, L. Tu, Y. Xie, S. Xu and Z. Li, *Adv. Mater.*, 2023, **35**, 2211917.
16 H. Yang, Z. Fu, S. Wang, H. Liu, J. Zhou, K. Wang, X. Wu, B. Yang, B. Zou and W. Zhu, *Mater. Adv.*, 2021, **2**, 4859–4866.
17 B. Yu, Y. Wang, L. Wang, X. Tan, Y. Zhang, K. Wang, M. Li, B. Zou and X. Zhang, *Phys. Chem.*, 2019, **21**, 17696–17702.
18 Y. Wang, X. Tan, Y. Zhang, S. Zhu, I. Zhang, B. Yu, K. Wang, B. Yang, M. Li, B. Zou and X. Zhang, *J. Am. Chem. Soc.*, 2015, **137**, 931–939.
19 X. Shi, N. Yan, G. Niu, S. H. P. Sung, Z. Liu, J. Liu, R. T. K. Kwok, J. W. Y. Lam, W. Wang, H. H. Y. Sung, I. D. Williams and B. Z. Tang, *Chem. Sci.*, 2020, **11**, 3152–3163.
20 J. Liu, W. Huang, B. Liang, Y. Chen, Y. Liu, X. Zhang, S. Zheng, L. Zhu, S. Feng and W. Huang, *Chem. Mater.*, 2022, **34**, 9492–9502.
21 P. Marandi, K. Naim, K. Parida and P. P. Neelakandan, *ACS Mater. Lett.*, 2022, **4**, 2499–2505.
22 X. Zheng, X. Liu, L. Liu, X. Li, S. Jiang, C. Niu, P. Xie, G. Liu, Z. Cao, Y. Ren, Y. Qin and J. Wang, *Angew. Chem., Int. Ed.*, 2022, **61**, e202113073.
23 Y. Takeda, T. Kaihara, M. Okazaki, H. Higginbotham, P. Data, N. Tohnai and S. Minakata, *Chem. Commun.*, 2018, **54**, 6847–6850.
24 Z. Wang, F. Yu, W. Chen, J. Wang, J. Liu, C. Yao, J. Zhao, H. Dong, W. Hu and Q. Zhang, *Angew. Chem., Int. Ed.*, 2020, **59**, 17580–17586.
25 H. Traeger, Y. Sagara, D. J. Kiebala, S. Schrettl and C. Weder, *Angew. Chem., Int. Ed.*, 2021, **60**, 16191–16199.
26 Y. Aoyama, S. Ito and K. Tanaka, *Macromolecules*, 2024, **57**, 6559–6567.
27 Y. Ge, Y. Wen, H. Liu, T. Lu, Y. Yu, X. Zhang, B. Li, B. Zhang, W. Li and B. Yang, *J. Mater. Chem. C*, 2020, **8**, 11830–11838.
28 W. Tao, L. Zhang, J. Gong, J.-X. Zhang, K. Wang, X. Jiang, X. He and P. Wei, *Dyes Pigm.*, 2023, **210**, 110967–1109774.
29 W. Shi, B. Rong, S. Li, Y. Lin, Y. Liao, C. Cao, S. Pan and B. Wei, *J. Mol. Struct.*, 2024, **1308**, 138050.

30 C. Zhu, Q. Luo, Y. Shen, C. Lv, S. Zhao, X. Lv, F. Cao, K. Wang, Q. Song, C. Zhang and Y. Zhang, *Angew. Chem., Int. Ed.*, 2021, **60**, 8510–8514.
31 M. Yamaguchi, S. Ito, A. Hirose, K. Tanaka and Y. Chujo, *J. Mater. Chem. C*, 2016, **4**, 5314–5319.
32 H. Zhang, Y. Nie, J. Miao, D. Zhang, Y. Li, G. Liu, G. Sun and X. Jiang, *J. Mater. Chem. C*, 2019, **7**, 3306–3314.
33 D. F. Xu, J. Y. Hao, H. Z. Gao, Y. H. Wang, Y. Wang, X. L. Liu, A. X. Han and C. Zhang, *Dyes Pigm.*, 2018, **150**, 293–300.
34 W. Yang, Y. Yang, Y. Qiu, X. Cao, Z. Huang, S. Gong and C. Yang, *Mater. Chem. Front.*, 2020, **4**, 2047–2053.
35 L. Shen, C. J. Yu, H. F. Xie, N. Xu, H. Xu, Y. L. Huang, C. Redshaw, X. Feng and Q. L. Zhan, *Mater. Chem. Front.*, 2022, **6**, 2491–2498.
36 J. Jiang, C. Hu, J. Liu, L. Ma, Y. Wang and J. Guo, *J Alloy. Compd.*, 2024, **1008**, 176594.
37 H. Yao, Y. Cui, R. Yu, B. Gao, H. Zhang and J. Hou, *Angew. Chem., Int. Ed.*, 2017, **56**, 3045–3049.
38 Y. Liu, Q. Zeng, B. Zou, Y. Liu, B. Xu and W. Tian, *Angew. Chem., Int. Ed.*, 2018, **57**, 15670–15674.
39 W. Cui, C. Liu, X. Chao, M. Xie, Q. Sun, D. Liu, Y. Pan, S. T. Zhang, S. Xue and W. Yang, *Adv. Opt. Mater.*, 2023, **11**, 2202947.
40 Z. Chen, Z. Xu, T. Qin, D. Wang, S. Zhang, T. Lv, L. Wang, X. Chen, B. Liu and X. Peng, *Sens. Actuators, B*, 2024, **398**, 134687.
41 X. Han, D. Sun, S. Tang, Y. Wu, L. Wang, X. Zhang and S. Liu, *J. Mater. Chem. C*, 2021, **9**, 17307–17312.
42 M. Yang, I. S. Park, Y. Miyashita, K. Tanaka and T. Yasuda, *Angew. Chem., Int. Ed.*, 2020, **59**, 13955–13961.
43 Q. Qi, C. Li, X. Liu, S. Jiang, Z. Xu and R. Lee, *J. Am. Chem. Soc.*, 2017, **139**, 16036–16039.
44 C. Mongin, A. M. Ardoy, R. Méreau, D. M. Bassani and B. Bibal, *Chem. Sci.*, 2020, **11**, 1478–1484.
45 X. C. Hu, F. B. Liu, X. Z. Zhang, Z. Y. Zhao and S. M. Liu, *Chem. Sci.*, 2020, **11**, 4779–4785.
46 S. Haldar, D. Chakraborty, B. Roy, G. Banappanavar, K. Rinku, D. Mullangi, P. Hazra, D. Kabra and R. Vaidhyanathan, *J. Am. Chem. Soc.*, 2018, **140**, 13367–13374.
47 K. Yuhara and K. Tanaka, *Angew. Chem., Int. Ed.*, 2024, **63**, e202319712.
48 J. Yang, X. Hu, M. Fan and S. Liu, *Org. Chem. Front.*, 2023, **10**, 422–429.
49 C. Xu, T. Li, J. Miao, K. Liu, Y. Nie, G. Liu and X. Jiang, *New J. Chem.*, 2023, **47**, 4448–4457.
50 Y. Zhan, *Dyes Pigm.*, 2020, **173**, 108002.
51 J. Miao, Z. Zhang, Z. Cui and M. Zhang, *Mater. Adv.*, 2022, **3**, 2692–2696.
52 Y. Chen, A. Li, X. Li, L. Tu, Y. Xie, S. Xu and Z. Li, *Adv. Mater.*, 2023, **35**, 2211917.
53 Y. Chen, X. Li, W. Che, L. Tu, Y. Xie and Z. Li, *J. Mater. Chem. C*, 2021, **9**, 11738–11744.
54 W. W. Xu, Y. X. Qin, J. Niu, W. Xu, Y. Chen, H. Y. Zhang and Y. Liu, *Adv. Opt. Mater.*, 2023, **11**, 2202431–2202441.
55 J. Yang, X. Hu, M. Fan and S. Liu, *Org. Chem. Front.*, 2023, **10**, 422–429.
56 Y. Qi, N. Ding, Z. Wang, L. Xu and Y. Fang, *ACS Appl. Mater. Interfaces*, 2019, **11**, 8676–8684.
57 Y. Gu, Z. Zhao, H. Su, P. Zhang, J. Liu, G. Niu, S. Li, Z. Wang, R. T. K. Kwok, X. L. Ni, J. Sun, A. Qin, J. W. Y. Lam and B. Z. Tang, *Chem. Sci.*, 2018, **9**, 6497–6502.
58 T. Sun, L. Wei, T. Zhai and F. Zhao, *Dyes Pigm.*, 2023, **220**, 111663–111669.